

# Diurnal and Longitudinal Variations in the Equatorial Anomaly for Winter Solstice According to Interkosmos-19 Satellite Data

A. T. Karpachev\*

*Pushkov Institute of Terrestrial Magnetism, Ionosphere, and Radio Wave Propagation,  
Russian Academy of Sciences (IZMIRAN), Troitsk, Moscow, 108840 Russia*

\*e-mail: karp@izmiran.ru

Received March 23, 2020; revised April 13, 2020; accepted May 21, 2020

**Abstract**—The equatorial anomaly dynamics in the winter solstice is studied based on data from topside sounding of the ionosphere from the Interkosmos-19 satellite for high solar activity. This is the final study on the construction of the pattern of equatorial anomaly variations under conditions of high solar activity. Changes in the equatorial anomaly structure with local time and longitude are considered in detail. It is shown that the anomaly begins to form at ~0800 LT during the creation of the winter northern crest, but the well-developed equatorial anomaly is formed only by 1000–1100 LT. The daytime maximum of the equatorial anomaly development is reached at 1200 LT. The  $f_oF2$  value above the equator and the degree of the equatorial anomaly development (equatorial anomaly intensity, EAI) at 1200 LT vary with longitude according to changes in the vertical plasma drift velocity  $W$ . Three harmonics are observed in the longitudinal variations in  $W$ ,  $f_oF2$ , and EAI at this time. The EAI increases up to the diurnal maximum 1.5–2.0 h after the evening  $W$  burst. Longitudinal variations in  $f_oF2$  at 2000 LT are also associated with the relevant variations in  $W$ , in which two harmonics are revealed. The degree of equatorial anomaly development drops after the evening peak but equatorial anomaly is still well-developed at midnight and is completely absent at 0500–0700 LT. The EAI at different moments of local time differs rather strongly for different longitudinal sectors. The average position of northern crest is  $\sim 25^\circ$  of the geomagnetic inclination  $I$ , and the southern crest is at  $\sim -30^\circ I$ . During the day, the winter crest is higher than the summer crest; by night-time, it is quite the opposite. Thus, a well-expressed equatorial anomaly is observed from 1000–1100 to 0000–0200 LT during the winter solstice.

DOI: 10.1134/S0016793221010060

## 1. INTRODUCTION

This paper is dedicated to the study of the equatorial anomaly (EA) for the winter solstice. It completes the construction of a comprehensive pattern of EA variations in different seasons, since analyses of the EA in the period of equinoxes (Karpachev, 2018) and for summer conditions (Karpachev, 2020) were published earlier. Data from topside sounding on board the Interkosmos-19 (IK-19) were used in all of these studies. Until now, IK-19 has been the only satellite to record the global distribution of electron density, including the  $f_oF2$  and  $hmF2$  variations for high solar activity. The EA structure in  $f_oF2$  is studied in this paper based on IK-19 data averaged for the northern winter, i.e., for November–February. Thus, the data present a certain average pattern in the quiet ( $Kp < 3$ ) winter equatorial ionosphere for high solar activity. The obtained pattern presents rather thoroughly the diurnal and longitudinal-latitude variations in the EA structure, including variations of its crests and intensity. The creation of this pattern became possible after the processing of the entire data set of the IK-19

was completed. The preprocessing of these data requires a lot of time and effort; therefore, it has been performed on a regular basis only in recent years. With this processing, the resulting IK-19 data array made it possible to obtain the most complete EA pattern for high solar activity, even though the EA has been actively studied already for about 70 years. This is primarily associated with a lack of data in the equatorial ionosphere. Suffice it to say that the EA was studied for many years based on data from ground-based stations, mainly, in two longitudinal sectors, the Asian and American sectors, and, partially, in the African sector (Rao, 1963; Lyon and Thomas, 1963; Rao and Malthotra, 1964; Rastogi et al., 1972; Rajaram, 1977; Walker, 1981; Sastri, 1990). Several studies were conducted using the data of topside sounding on board the Alouette and ISIS satellites, the data from which were also recorded only in the Asian and American longitudinal sectors (Lockwood and Nelms, 1964; King et al., 1967; Rush et al., 1969; Eccles and King, 1969; Sharma and Hewens, 1976). Unfortunately, these studies refer mainly to low solar activity. The GPS total electron content (TEC) variations are also tied to

land and not directly related to the  $foF2$  variations; nevertheless, there is a detailed study of the EA diurnal variations for high solar activity in the Asian sector (Zhao et al., 2009) used below for comparison. Several satellites carried out in situ measurements of the electron density at fixed altitudes and provided a global view of equatorial ionosphere. This is especially true for the CHAMP satellite, the orbit of which was almost at altitudes of the  $F2$  layer maximum: 350–480 km (Liu et al., 2007; Lei et al., 2010). Finally, the data from the FORMOSAT-3/COSMIC experiment also cover a period with low solar activity. Nevertheless, they are of interest, since these data provide the  $foF2$  global distribution, which show the differences in the EA structure at different solar activities (Yue et al., 2015; Tsai et al., 2009; Ram et al., 2009).

## 2. OBSERVATIONAL DATA

The IK-19 satellite actively operated from March 1979 to February 1981. This period was characterized by high solar activity, with an average  $F10.7$  value of  $\sim 200$ . The satellite moved along the elliptic orbit at heights of 500–1000 km and an inclination of  $74^\circ$ . On board the satellite, there was a device that allowed digital ionograms to be recorded at any longitude within the limits of orbit inclination. The  $N(h)$  profiles of the topside ionosphere were calculated from these ionograms according to the Jackson technique (Jackson, 1969) to yield the  $foF2$  and  $hmF2$  values. These values were used to construct the distributions of the  $F2$ -layer maximum parameters in the EA region within the limits of  $\pm 70^\circ$  of the geomagnetic inclination  $I$ . November–February are ranked among the winter months, i.e., eight months for two years of satellite operation. Over this period, more than 40000 pairs of the  $foF2$  and  $hmF2$  values were obtained for quiet conditions  $Kp \leq 3$ . These data are quite enough for the construction of 12 so-called LT maps for each 2 h of local time, so that a single map accounts for 2200 to 3700 values of  $foF2$  or  $hmF2$ . The maps were constructed with the Surfer routine program using the inverse distance method. The data for each map uniformly covered all longitudes; therefore, a rather smooth distribution of  $foF2$  and  $hmF2$  was obtained and was additionally corrected during data analysis. Only  $foF2$  variations are considered in this paper.

## 3. DEVELOPMENT OF THE EQUATORIAL ANOMALY

Figure 1 presents the  $foF2$  distribution in the period of EA development, namely, for 0700–1400 LT, while Fig. 2 shows the latitudinal  $foF2$  profiles in the most characteristic longitudinal sectors: the Asian ( $90^\circ$ ) and American ( $300^\circ$ ) sectors. In the first, the geomagnetic equator is located as far north of geographic equator as possible, while, conversely, it is located as far south of it in the second sector. During the winter solstice, as

during the summer one, the winter EA crest is first formed. This is a well-known fact (Lyon and Thomas, 1963; Thomas, 1968), and it is clearly pronounced in both figures. This fact was disputed by Walker and Chen (1976), who detected an inverse asymmetry according to the Alouette-1 data in the Asian sector ( $105^\circ$ ) for high solar activity during December 1969–January 1970: during the day, the summer (southern) crest proved to be 8% higher and  $8^\circ$  DIP further from the equator. However, in a subsequent review (Walker, 1981) based on ground data, it was claimed that the winter crest develops earlier and is larger in magnitude in any solstice and in any longitudinal sector. The winter crest appears at 0800 LT for all longitudes at a latitude of  $\sim 20^\circ$  and at a latitude of  $5^\circ$  in the sector of  $285^\circ$ . Over the course of time, the winter crest moves from the equator. It develops quickly from 0800 to 1000 LT and more slowly from 1000 to 1200 LT. At 1400 LT, the winter crest is higher than at 1200 LT at some longitudes and lower at others, but, on average, the situation remains stable for the entire daytime. In a review (Rajaram, 1977) based on ground-based data in the Asian sector for high solar activity, it was shown that the winter crest is always higher than the summer one. A strong asymmetry of crests was also observed in the African sector in comparison with that in the American sector (Thomas, 1968). However, the EA asymmetry is not expressed very clearly in Fig. 2 in either the Asian or the American sector. A not very strong asymmetry was also obtained from the GPS TEC data in the longitudinal sector of  $120^\circ$  by Zhao et al. (2009).

The situation in the Southern hemisphere is more complicated. At 0700 LT, the electron density in the Southern hemisphere is higher than in Northern hemisphere under the action of solar ionization; therefore, the southern crest forms against a higher background level. At 0800 LT in the Southern hemisphere, the  $foF2$  maximum is observed at  $-(40^\circ-50^\circ)$ , which is not related to the EA, since it is located far enough in the latitude for a normal EA crest created by the fountain effect. As a result, the  $foF2$  minimum turns out to be offset to the Southern hemisphere and is not an equatorial trough of ionization associated with EA (Fig. 2). At 1000 LT, the position of the  $foF2$  maximum corresponds to the northern crest position only at longitudes of  $180^\circ-270^\circ$ . At the other longitudes in the Southern hemisphere, this maximum as before is located too far from the equator (Fig. 2). By 1200 LT, the southern summer crest develops intensively and almost equals the northern winter crest in magnitude. In the Asian longitudinal sector, it is similarly very distant from the equator, but it is now associated with the very strongly developed anomaly, as shown in Fig. 1. The situation for 1400 LT is, on principle, no different from that for 1200 LT. It is also confirmed by the Alouette-1 data, according to which the summer southern crest at the longitudes of Singapore on December 2, 1962, at 1405 LT was at  $-40^\circ I$ , while

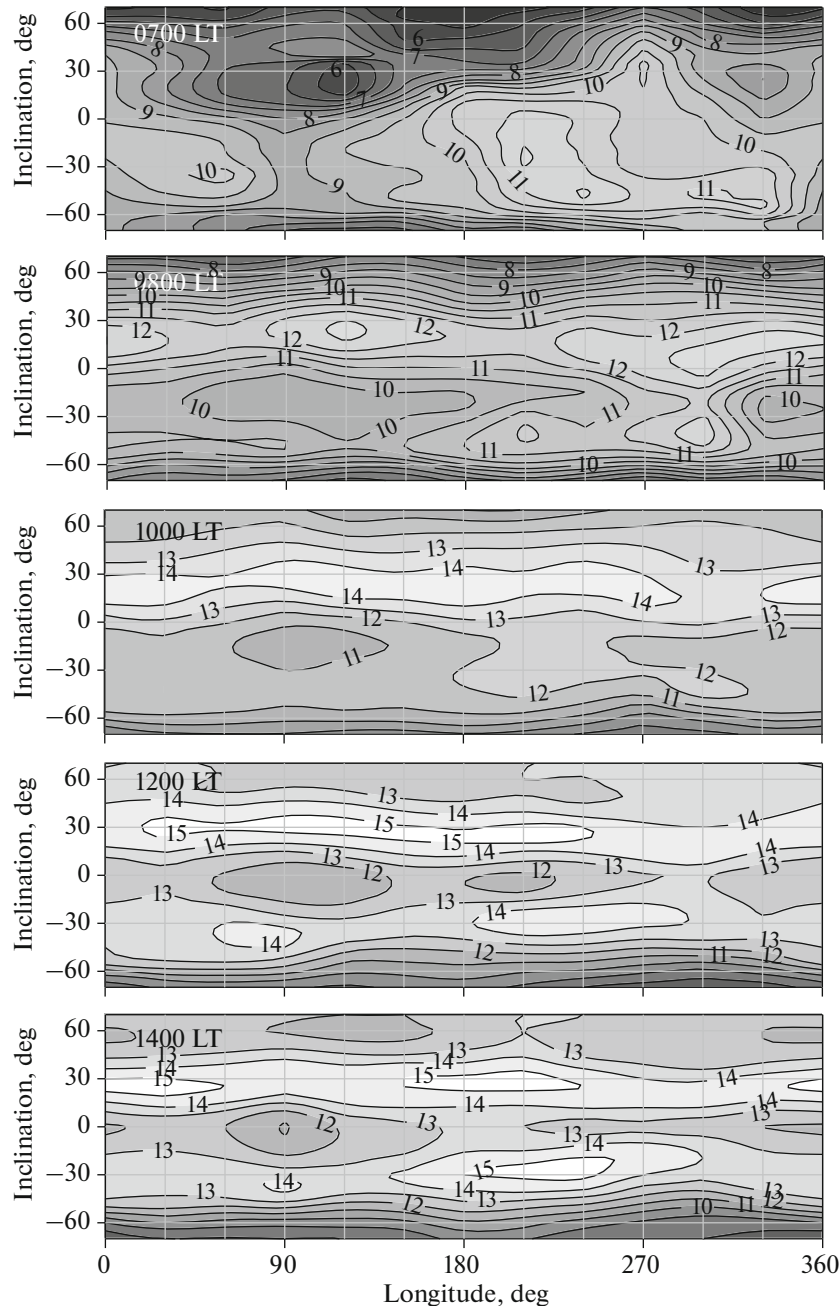
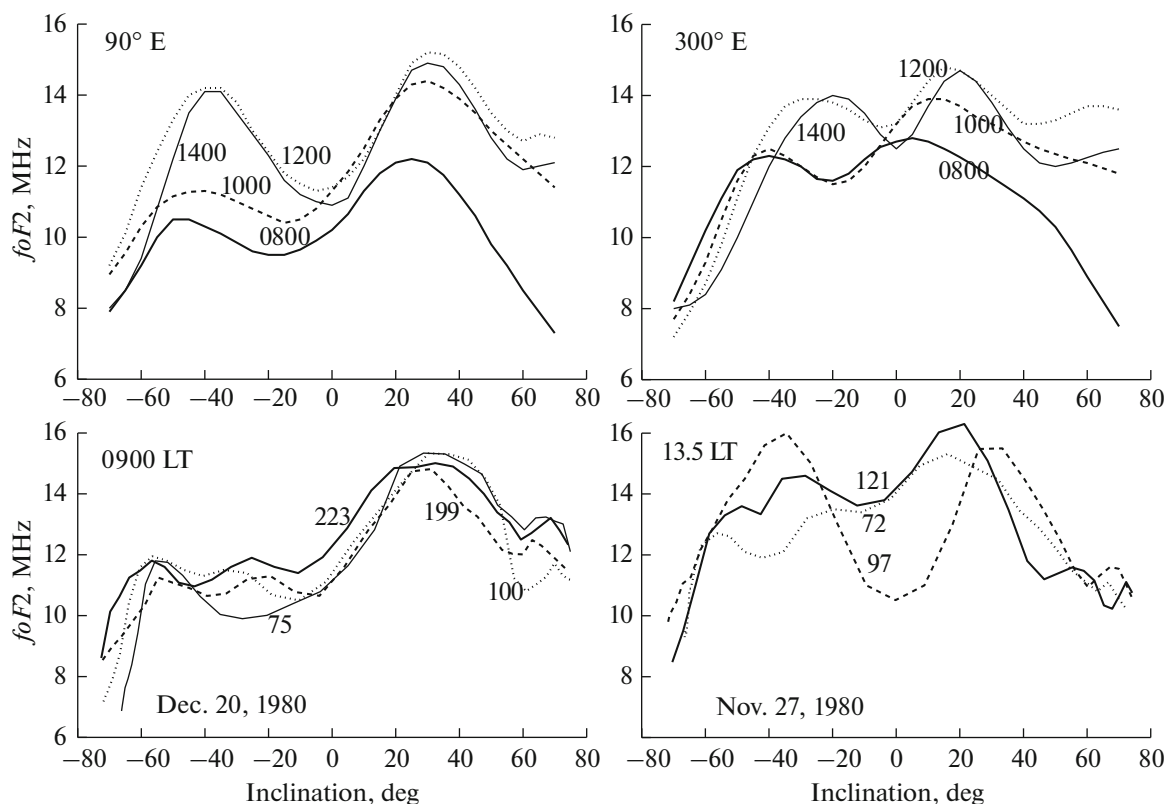


Fig. 1. Distribution of  $foF2$  (LT maps) in the period of EA development for 0700, 0800, 1000, 1200, and 1400 LT.

it was at the latitude of  $-10^\circ I$  in the longitudinal sector of  $75^\circ W$  (King et al., 1967).

It can be assumed that the  $foF2$  maximum in the Southern hemisphere is formed by the joint action of the vertical plasma drift, neutral wind, and solar ionization. In other words, the southern crest forms on the background of the midlatitude  $foF2$  maximum. This can be easily seen in Fig. 2. The upper panel of Fig. 2 shows the averaged, smoothed latitudinal  $foF2$  profiles. The lower panel shows the individual satellite flights at different longitudes in the morning (Decem-

ber 20, 1980) and afternoon (November 27, 1980) ionosphere (the local time on the equator was 0900 and 1330 respectively). It can be seen that a single, higher-latitude  $foF2$  maximum is recorded in the morning in the Southern hemisphere on some flights, while another (low-latitude) maximum is recorded on other flights. The low-latitude maximum is approximately at the latitudes of the northern EA crest and is probably the southern EA crest, which is created by the fountain effect. However, this maximum is smoothed with averaging. At 1330 LT, a similar situation is



**Fig. 2.** Top: averaged latitudinal variations in  $foF2$  for 0800, 1000, 1200, and 1400 LT in the most characteristic longitudinal sectors of 90° and 300°. Bottom: individual satellite flights at different longitudes in the morning ionosphere on December 20, 1980, and in the afternoon ionosphere on November 27, 1980.

observed in the Asian sector. Thus, the southern summer crest begins to form at ~0900 LT, but it is masked out before midday by the more powerful high-latitude  $foF2$  maximum. The situation with the summer southern crest is very similar to the situation with the summer northern crest in the period of summer solstice (Karpachev, 2020).

In the literature, there are no other  $foF2$  data for winter conditions at high solar activity to confirm this conclusion. Only with the GPS TEC data obtained in the longitudinal sector of 120° for  $F10.7 > 150$  can the EA dynamics be traced for winter conditions (Zhao et al., 2009). In Fig. 5 of the mentioned study, it can be seen that the winter northern crest begins to form at ~0900 LT, while the southern summer crest starts to form slightly later, from 1000–1100 LT. In this case both crests are almost symmetrical relative to the geomagnetic equator, and, consequently, the higher-latitude maximum of the electron density is not observed.

At low solar activity, the summer crest begins to form in the Asian sector from 0700–0800 LT at latitudes of 10°–20°  $I$  according to data obtained from the night sky glow (King, 1968). However, according to the Alouette-1 data for the Singapore longitudes on December 2, 1962, the summer crest at 1405 LT was at the same latitude of ~40°  $I$  as in Fig. 2 (King et al.,

1967). Accordingly, the EA begins to reveal itself at 0800–0900 LT from the data of Alouette-1 in the American sector (Sharma and Hewens, 1976). The EA dynamics was traced in detail (for each hour) with the FORMOSAT-3/COSMIC data for low solar activity (January–February, 2007) (Ram et al., 2009). From Fig. 2 of the mentioned paper, it can be seen that the winter crest begins to appear at 0800–0900 LT, while the summer crest begins to appear only at 0900–1000 LT. The winter crest at all longitudes forms at 0900–1000, while both crests form in the period of 1000–1100 LT. In summary, it can be concluded that the EA with two crests begins to manifest itself at 0900–1000 LT under winter conditions, while the clearly pronounced EA appears at 1000–1100 LT.

As for the dynamics of the development of the summer anomaly crest against the background of the midlatitude  $foF2$  maximum, then this issue should be considered in more detail, both experimentally and theoretically.

By midday, the EA is best developed at longitudes of 90°–120° in comparison with other longitudes. As for the delay in EA development at the longitudes of America, it has been noted in many early studies. However, they mainly refer to low solar activity and/or to the equinox (e.g., Lyon and Thomas, 1963; Hop-

kins, 1972; Sharma and Hewens, 1976; Rajaram, 1977). Analysis of Figs. 1 and 2 shows that the EA develops more weakly in the American longitudinal sector, but it cannot be said based on the IK-19 data that it forms later.

The  $foF2$  variations with longitude on the geomagnetic equator were revealed for the first time from the IK-19 data (Karpachev, 1988). On the upper and middle panels of Fig. 3, respectively, the solid curve shows the longitudinal  $foF2$  variations above the equator and the degree of EA development, which is denoted by the accepted term “equatorial anomaly intensity” (EAI). The degree of EA development was defined as the ratio of  $foF2$  in the winter crest maximum to  $foF2$  in the equatorial trough, i.e.,  $EAI = foF2_C / foF2_E$ . Variations in both parameters are obtained by averaging of the data for 1200 LT and are presented in Fig. 3 with a step of  $30^\circ$  in longitude. For comparison, the longitudinal variations in the vertical plasma drift velocity  $W$  above the equator in the period of EA development are also presented (dashed curve). They were obtained from the ROCSAT-1 satellite data for winter (November–February) quiet conditions in 1999–2004 for high solar activity ( $F10.7 > 180$ ) (Kil et al., 2009).

The diurnal pattern of vertical drift is the same for the whole winter, with only amplitude changes from month to month. Therefore, the drift velocity variations in Fig. 3 for December were chosen for comparison; they were taken from the colored plot in Fig. 5 of Kil et al. (2009). Two minima and two maxima are observed in them. The maximum at  $210^\circ$  began at 0900 LT, reached the highest values at 1000–1100 LT, and was sharply reduced by 1200 LT. The weaker maximum at  $120^\circ$  began from about 1030 LT and reached the highest values at 1200 LT. As a result, this weaker maximum caused a stronger drop in  $foF2$  above the equator at 1200 LT than the second one (axis  $Y$  for  $foF2$  is reversed in Fig. 3). (The second  $foF2$  minimum at longitudes of  $180^\circ$ – $240^\circ$  manifested itself still much more weakly at 1400 LT). Due to the different time delay, a full correspondence between  $foF2$  and  $W$  cannot be expected. Nevertheless, the observed agreement between them is rather high; in any case, the extrema almost coincide. This fully applies also to EAI variations. They are similar to  $foF2$  variations, which means that the EAI is determined mainly by the  $foF2$  variations above the equator, which, in turn, are determined by variations in the velocity of the vertical plasma drift. This is a well-known fact; only the high agreement of all of the considered quantities, despite the different time delay between the drift and EA parameters, is a surprise. We also note that the third harmonic dominates during winter in longitudinal variations of all parameters, as opposed to summer and equinox, when a strong fourth harmonic is observed in the daytime (Fejer et al., 2008; Oh et al., 2008; Ram et al., 2009; Huang et al., 2010).

The bottom panel in Fig. 3 shows the longitudinal variations in the position of the northern and southern

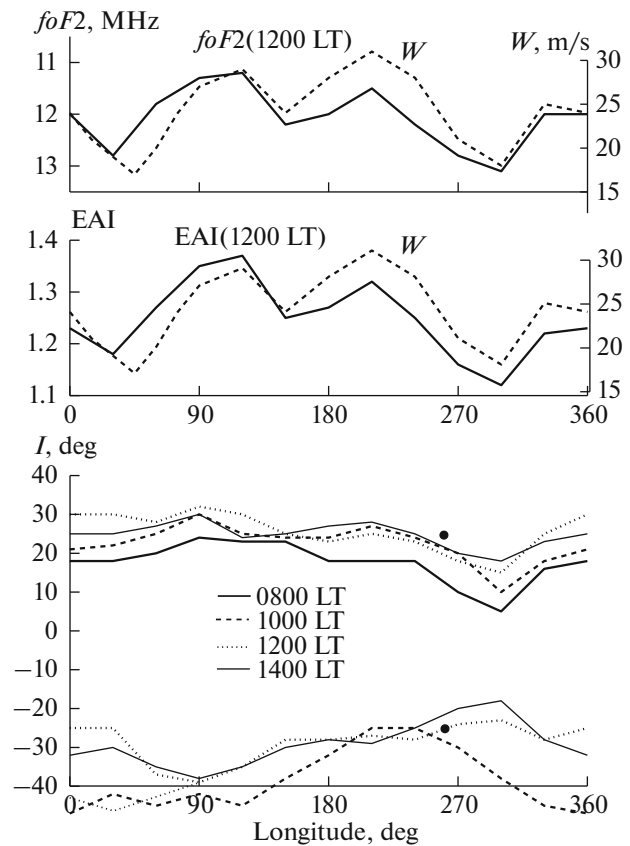


**Fig. 3.** Top: longitudinal variations in  $foF2$ , EAI, and the vertical plasma drift velocity  $W$  (Kil et al., 2009). Bottom: longitudinal variations in the position of EA crests for different hours of local time. Dots indicate the crest positions according to the Alouette data for midday (Sharma and Hewens, 1976).

EA crests for 0800–1400 LT. Their dynamics in the period of EA development, in fact, was already discussed above. First, the winter EA crest appears at 0800 LT. Its position strongly changes with longitude (from  $5^\circ I$  to  $24^\circ I$ ); the average value is  $\sim 18.5^\circ I$ . From 0800 to 1000 LT, the crest strongly increases in magnitude and moves away from the equator by  $\sim 5^\circ I$ . The development of winter crest then slows; it moves away from the equator before 1200 LT just by  $2.5^\circ I$  and actually stabilizes, since its average position before 1400 LT is unchanged, while the difference in longitudinal variations between 1200 and 1400 LT is actually within the limits of the accuracy of the determination of the maximum crest positions.

The summer, i.e., southern, crest begins to manifest itself only at 1000 LT and only at longitudes of  $210^\circ$ – $240^\circ$ . The  $foF2$  maximum, which is shown for 1000 LT by the solid continuous curve, is not the EA crest for the other longitudes, since, as can be clearly seen now, it is located too far from the equator for a “normal” crest. This maximum at the longitudes of  $00^\circ$ – $60^\circ$  was recorded even at 1200 LT, which is shown

by the curved segment in Fig. 3. The “normal” summer crest for all longitudes formed only by 1200 LT.

Thus, the EA with two developed crests forms only by midday. At this time, the  $foF2$  value in EA crests reaches maximum values of 14–15 MHz and remains unchanged for the entire daytime period. The average position of northern crest at midday is  $\sim 25^\circ$ , while that for the southern crest is  $\sim 30^\circ$ ; thus, the asymmetry of EA crests in the period of winter solstice in both position and magnitude (Fig. 2) is more moderate than strong. Consequently, the equatorial trough in  $foF2$  is shifted by a few degrees into the Southern hemisphere.

The EA crests are most distant from the equator in the longitudinal sector of  $90^\circ$ , while they are closest in the longitudinal sector of  $270^\circ$ . Accordingly, the most developed EA is in the Asian sector, while the least developed EA is in the American sector. The total width of EA crests at 1200–1400 LT in terms of magnetic declination reaches  $\sim 70^\circ I$  in the longitudinal sector of  $90^\circ$  and only  $40^\circ I$  in the longitudinal sector of  $300^\circ$ . According to the Alouette satellite data for the American sector ( $90^\circ$ – $55^\circ W$ ) for low solar activity in winter, both EA crests were located at the latitude of  $\sim 25^\circ$  (Sharma and Hewens, 1976). This exactly corresponds to the southern crest at midday and with distance from the equator in the Northern hemisphere in the same sector in Fig. 3.

There is no other  $foF2$  data for high solar activity for comparison with the midday data of IK-19 in Fig. 1. However, there is an ion density  $Ni$  distribution obtained for the December solstice,  $F10.7 = 200$ , 1300 LT; it is presented in Fig. 9 of Chen et al. (2016). This distribution was obtained from the ROCSAT-1 satellite data at the rather high altitude of 600 km; nevertheless, it is consistent quite well with the  $foF2$  distribution for 1200 LT in Fig. 1. The ROCSAT-1 data show the most developed EA at longitudes of  $180^\circ$ – $210^\circ$ , a slightly less developed EA at longitudes of  $90^\circ$ – $120^\circ$ , and the least developed EA at  $30^\circ$ – $60^\circ$  and  $300^\circ$ . We note that longitudinal variations of the anomaly crests, according to the IK-19 and ROCSAT-1 data, are also very similar.

There is another  $Ni$  distribution obtained for winter midday conditions of high solar activity from data of the CHAMP satellite at the altitude of 400 km (Liu and Watanabe, 2008). It is presented in Fig. 3 in the mentioned study in the form of deviations from the zonal-mean values, i.e., it presents the  $Ni$  variations with longitude. The comparison with longitudinal variations in  $foF2$  for 1200 LT in Fig. 1 shows that all maxima of the ionosphere plasma density, except for one, nearly coincide. Thus, both satellites show, in general, a similar EA structure for midday conditions under high solar activity.

Finally, there is a  $foF2$  distribution that can be directly compared with the distribution for 1200 LT in Fig. 1. It was obtained from the COSMIC data, but it refers to low solar activity  $F10.7 = 76.4$  (Zeng et al.,

2008). It is interesting to note that this  $foF2$  distribution is in good agreement with Fig. 1 in the Western hemisphere but demonstrates worse agreement in the Eastern hemisphere, since it shows the maximum developed EA at  $150^\circ$ , not at  $90^\circ$ – $120^\circ$ . Whether this disagreement is associated with the difference in the EA structure for high and low solar activity or is explained by drawbacks of data arrays remains to be ascertained.

#### 4. EVENING ENHANCEMENT OF EQUATORIAL ANOMALY

When the EA reaches a local maximum at 1200 LT, it is in a relatively stable state for a few hours. The situation quickly changes in evening hours. Figure 4 shows the  $foF2$  distribution for the afternoon/evening hours of local time (1600, 1800, 2000, and 2200 LT); Fig. 5 presents the latitudinal  $foF2$  profiles for these time moments in the characteristic longitudinal sectors, while Fig. 6 depicts the variations in the EA parameters with longitude. We can trace the EA dynamics in evening hours by these plots. The  $foF2$  distribution at 1600 LT almost does not differ from the midday distribution. The electron density at crest maxima remains constant: 14–15 MHz; the EA is more strongly developed in the Asian sector and the less strongly developed in the American sector. At 1800 LT, rearrangement of the EA structure begins. The electron density at low/middle latitudes decreases by evening with a reduction in the ionosphere illumination; therefore, the anomaly crests become narrower. The electron density above the equator remains high; therefore, the EA at 1800 LT is slightly less developed than at midday.

After the evening (1800–1900 LT) burst of the vertical plasma drift, there is a sharp EA intensification that is clearly pronounced at 2000 LT. The electron density in crests and at middle latitudes still falls a little with a decrease in the solar illumination. However, above the equator, it strongly reduces under the action of the fountain effect, and the anomaly crests become even narrower, while the EAI reaches the maximum. The EA, as before, is most strongly developed in the Asian sector of  $90^\circ$ , less strongly in the American sector of  $300^\circ$ , and least developed in the longitudinal sector of  $210^\circ$ ; therefore, these longitudinal sectors are presented in Fig. 5. All of this can be clearly seen from Figs. 5 and 6.

The top panel in Fig. 6 shows the longitudinal  $foF2$  variations above the equator, in the EAI for 2000 LT, and in the vertical plasma drift velocity  $W$ . The  $W$  variations were obtained from the ROCSAT-1 data at high solar activity ( $F10.7 = 200$ ) for winter conditions during the evening burst of drift (1800–1900 LT) (Fejer et al., 2008). From Fig. 6 it can be seen that, as in the period of EA morning development, the longitudinal variations in  $foF2$  and EAI are generally determined by variations in the vertical plasma drift veloc-



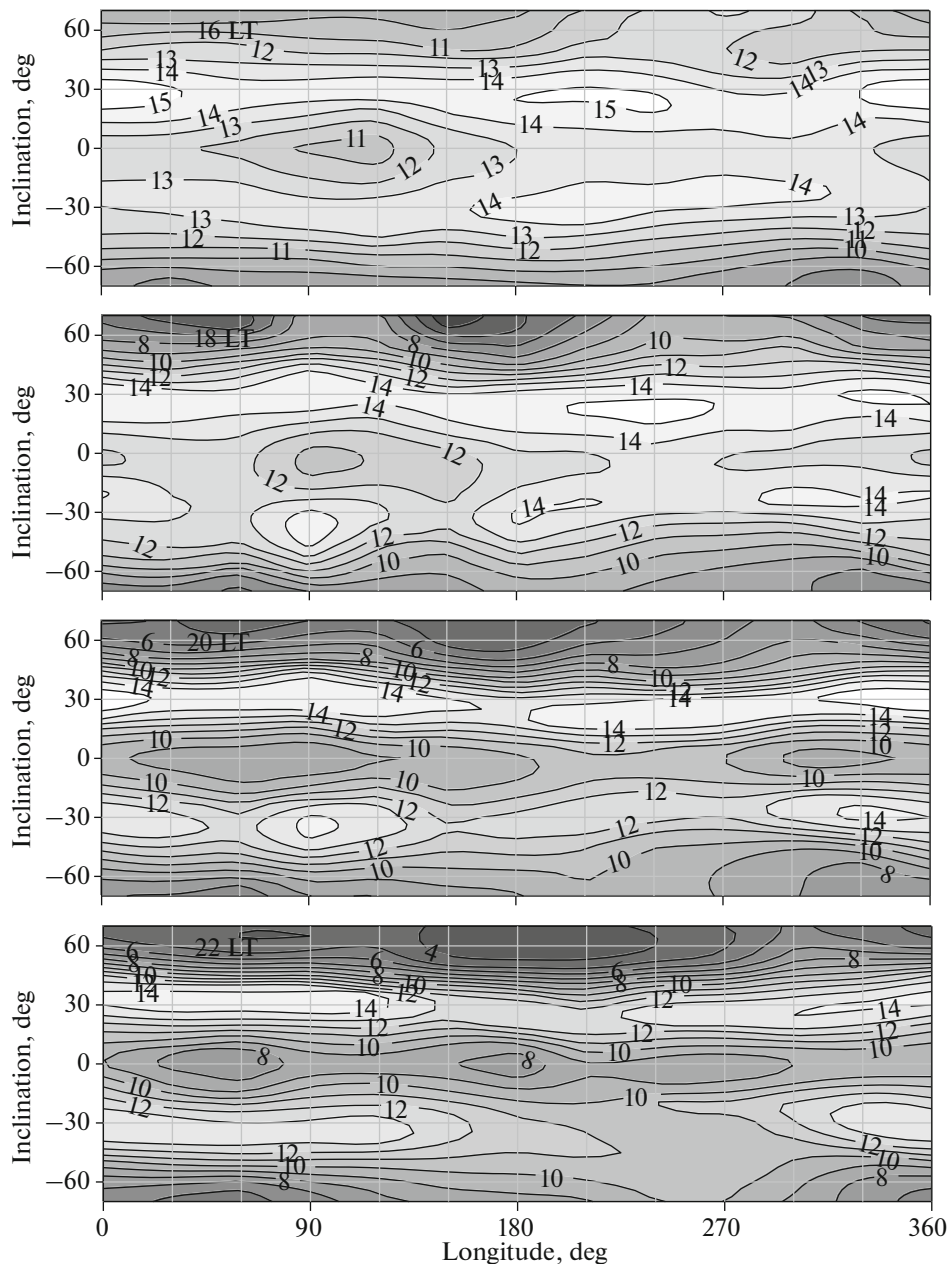
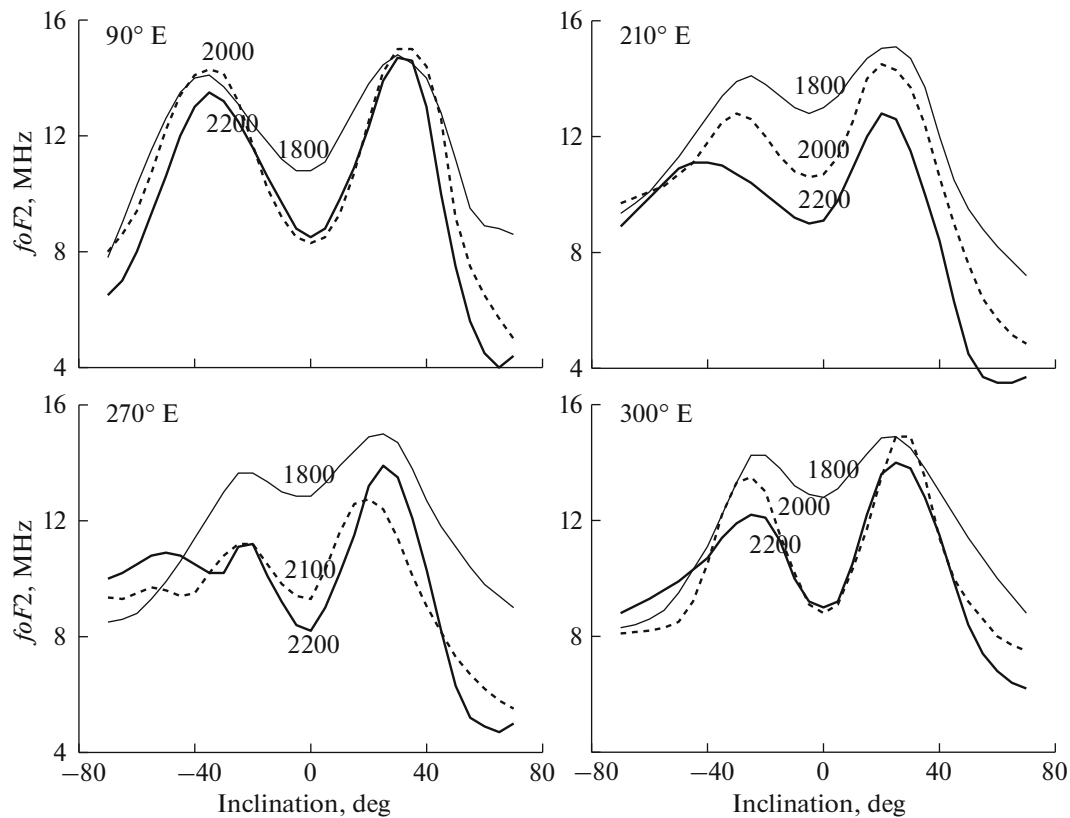


Fig. 4. Distribution of  $foF2$  for 1600, 1800, 2000, and 2200 LT.

ity. In any case, the extrema are close in longitude. In this case two harmonics are explicitly manifested in the EA parameters. The correlation of these parameters is not complete; the distinction is explicitly related to the presence of the strong first harmonic in the EA variations. It is inappropriate to discuss the origin of this harmonic until there is a confidence that it is not associated with drawbacks in measurements of the equatorial ionospheric parameters.

The bottom panel in Fig. 6 depicts the longitudinal variations in a position of crests for 2000, 2100, and 2200 LT. As should be expected, both crests are

located at the maximal distance from the equator ( $33^\circ I$ – $35^\circ I$ ) in the sector of  $90^\circ$ , where the EA is most developed, and as close as possible to the equator ( $20^\circ I$ – $22^\circ I$ ) at longitudes of  $210^\circ$ – $270^\circ$ , where the EA is weakly developed. The northern crest shows stable behavior in the evening hours. The southern crest behavior is much more complicated, as can be seen from Figs. 5 and 6. It is determined by formation of the so-called Weddell Sea anomaly (WSA) in the summer southern Hemisphere in the American sector. This anomaly was first discovered in the form of the night maximum of  $foF2$ , which exceeds the relatively low daytime values (Bellchambers and Pigott, 1958). The



**Fig. 5.** Latitudinal  $foF2$  variations for 1800, 2000, and 2200 LT in the most characteristic sectors of  $90^\circ$ ,  $210^\circ$ ,  $270^\circ$ , and  $300^\circ$ . In the longitudinal sector of  $270^\circ$ , the profile is given for 2100 LT instead of 2000 LT.

WSA has been studied intensely in recent years based on the IK-19 data too (Karpachev et al., 2011; Klimenko et al., 2015). The WSA begins to manifest itself as the second  $foF2$  peak at 2100 LT in the longitudinal sector of  $270^\circ$  (Fig. 5). Accordingly, this second peak is marked also in Fig. 6 for 2100 and 2200 LT. Moreover, the  $foF2$  maximum changes its position by a jump at 2200 LT.

We note that, the winter crest always remains higher than the summer one during both the day and evening and that the largest asymmetry is observed in the sector of  $270^\circ$ .

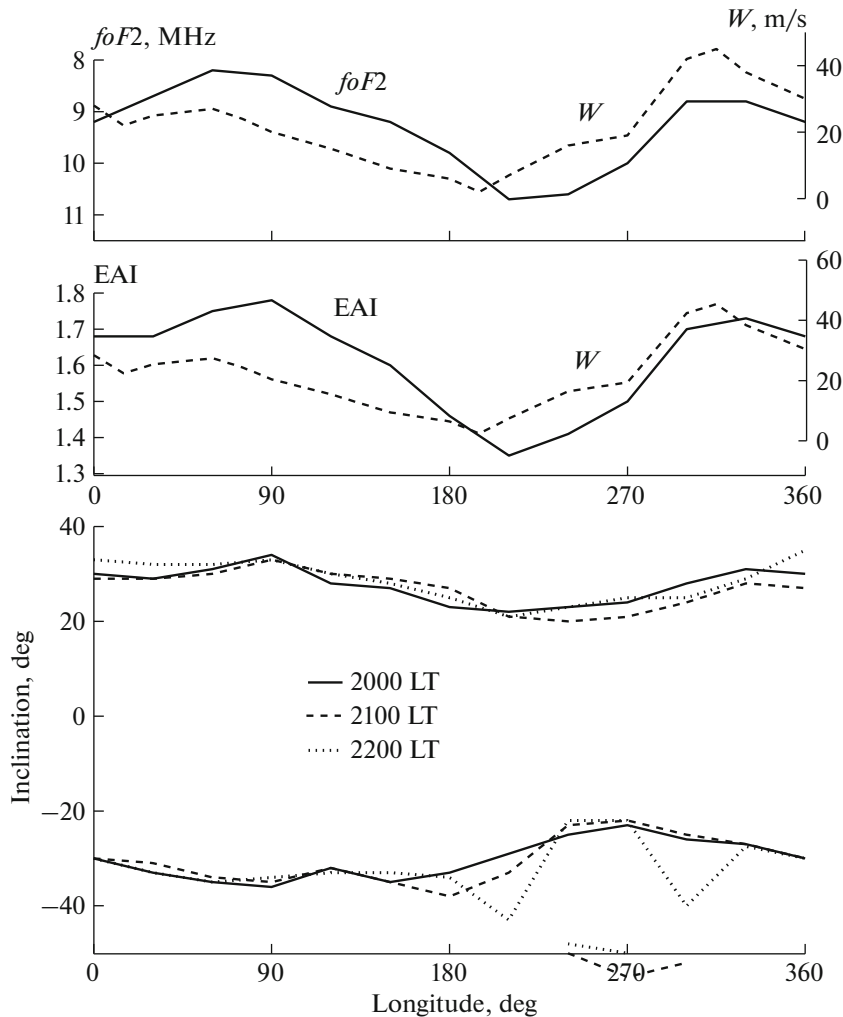
### 5. EQUATORIAL ANOMALY DECAY

Figure 7 shows the distributions of  $foF2$  for 0000, 0200, and 0400 LT, while Fig. 8 presents the latitudinal variations in  $foF2$  for these hours of local time in different longitudinal sectors. The  $foF2$  profiles for 2000 LT are given for comparison. In the period of EA decay, the electron density at all latitudes of the unlit equatorial ionosphere drops due to recombination. The vertical plasma drift changes direction: the downward drift drives the ionospheric plasma along the field lines from the high altitudes to the low ones (Balan and Bailey, 1995). The result of this process

depends on the solar activity. At low solar activity, the plasma deposit in the plasmasphere is small and is depleted rapidly; the EA decays immediately after the evening burst of vertical drift (Balan and Bailey, 1995). At high solar activity, the plasma deposit is sufficient for the downward drift to support the EA crests at a high level for a long time. This is the situation observed in Fig. 7: it is seen that a rather well-developed EA exists even at midnight.

The recombination effect is clearly seen in Fig. 8: after the EA development maximum at 2000 LT, the electron density abruptly drops at all latitudes, stronger in crests and weaker above the equator. After midnight, the rapid EA decay continues; the winter northern crest in this case decays much faster than the southern one, i.e., an asymmetry that is the reverse of that observed during the EA development forms. This is a well-known fact, which as revealed as early as in 1968 (Thomas, 1968). It is explained by the action of the meridional wind: in the daytime, the wind accelerates diffusion in the direction of the winter crest, while the wind increases the recombination at night, since it carries plasma down to the lower altitudes. Nevertheless, the least developed EA exists almost at all longitudes as early as at 0200 LT, excluding the longitudinal





**Fig. 6.** Top: longitudinal variations in  $foF2$  and EAI for 2000 LT, and the vertical plasma-drift speeds  $W$  (Fejer et al., 2008) for 1800–1900 LT. Bottom: longitudinal variations in the position of EA crests for different hours of local time.

sector of  $210^\circ$ , where the winter crest is not clearly recorded.

The winter crest almost completely decays by 0400 LT. The situation in the summer Southern hemisphere is complicated, since, as shown above, it is associated with WSA development. In the longitudinal sector of  $180^\circ$ – $330^\circ$ , the second midlatitude  $foF2$  maximum (Fig. 8) forms beginning from 2100 LT. It is situated poleward of a normal crest. It is clearly pronounced at 0000 LT on the LT map (Fig. 7) and on the  $foF2$  latitudinal cross-sections at longitudes of  $210^\circ$  and  $270^\circ$  in Fig. 8. At 0400 LT in the longitudinal sector of  $270^\circ$  in the Northern Hemisphere at latitudes of the normal anomaly crest, a noticeable  $foF2$  maximum is recorded, and the southern crest is absent; against this low background, the  $foF2$  maximum associated with WSA clearly manifests itself. The dynamics of both  $foF2$  maxima in the Southern hemisphere is considered below.

The bottom panel in Fig. 9 shows variations in the EA crest positions in the period of its decay. During EA decay, the crests shift towards the equator and decreases in magnitude. This standard behavior is observed in the winter hemisphere: the northern crest shifts to the equator and decreases until its disappearance by 0400 LT. In the Southern Hemisphere, a complicated pattern is observed, though its interpretation is not very difficult. As in the Northern hemisphere, a “normal” crest of the anomaly is observed at midnight near the latitude of  $-25^\circ I$ . Beginning from a longitude of  $180^\circ$ , it is accompanied by the second midlatitude  $foF2$  maximum associated with the WSA. At 0200 LT, the southern crest, like the northern one, moves to the equator; however, at longitudes of  $180^\circ$ – $270^\circ$  at the intermediate latitude, the  $foF2$  maximum is observed as the sum of the anomaly crest and the WSA maximum. We note, however, that this becomes understandable only in the context of a total analysis of the

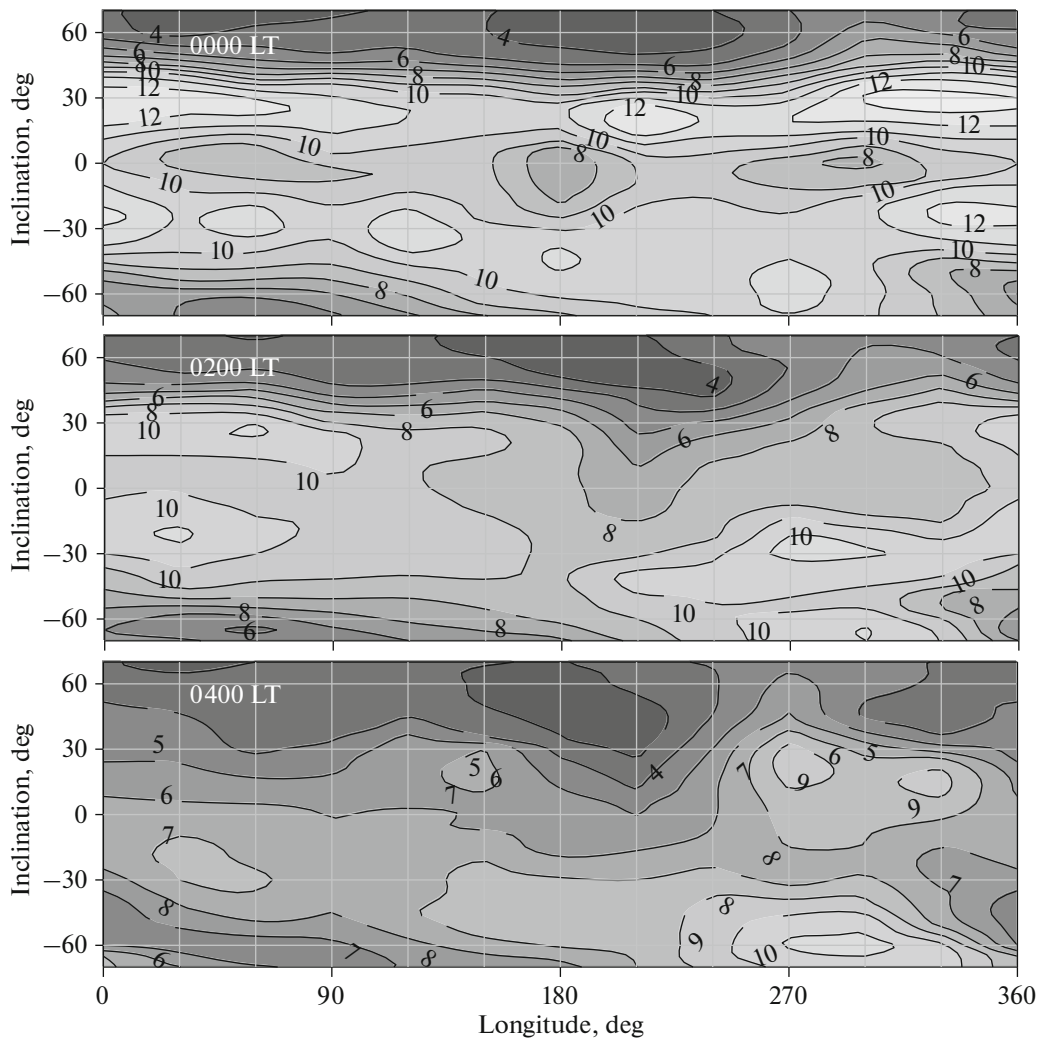


Fig. 7. Distribution of  $foF2$  for 0000, 0200, and 0400 LT.

equatorial ionosphere dynamics over the course of time.

Finally, the southern crest of anomaly during the movement to the equator degrades at 0400 LT and is even not observed in the Western hemisphere against the background of the  $foF2$  maximum formed by the WSA. This maximum at the longitudes of  $180^{\circ}$ – $330^{\circ}$  is always approximately at the same longitudes. However, interestingly, it is exiting at a latitude of  $32^{\circ} I$  in the longitudinal sector of  $60^{\circ}$ , i.e., the maximum at longitudes of  $60^{\circ}$ – $180^{\circ}$  is a sort of WSA extension. Since the main cause of WSA creation is a neutral wind, it is obviously the cause of this maximum formation.

In the longitudinal sector of  $90^{\circ}$ , the EA is the least developed at midnight in contrast to the rest of the day. After midnight, the anomaly crests monotonically shift to the equator, and the anomaly ceases to exist by 0400 LT. In the American sector, the EA, conversely, is the most developed at midnight. The winter crest

then rapidly decays, shifting to the equator. The anomaly dynamics in the Southern hemisphere is determined by the WSA. Finally, in the longitudinal sector of  $210^{\circ}$ , the EA also is rather well developed at midnight. However, at 0200 LT, the  $foF2$  maximum in the Southern hemisphere is most likely the sum of the midlatitude increase and the normal anomaly crest. However, it is difficult to consider it as anomaly development.

## 6. EQUATORIAL-ANOMALY DIURNAL VARIATIONS

The top panel in Fig. 10 presents the diurnal variations in the EAI. They were derived by averaging of the data separately for longitudes of  $90^{\circ}$ – $120^{\circ}$  and  $270^{\circ}$ – $300^{\circ}$ . Figure shows also the variations in the vertical plasma drift identified by Fejer et al. (2008) from the ROCSAT-1 data for winter conditions under high solar activity. The EA begins to form at 0800 LT. It is

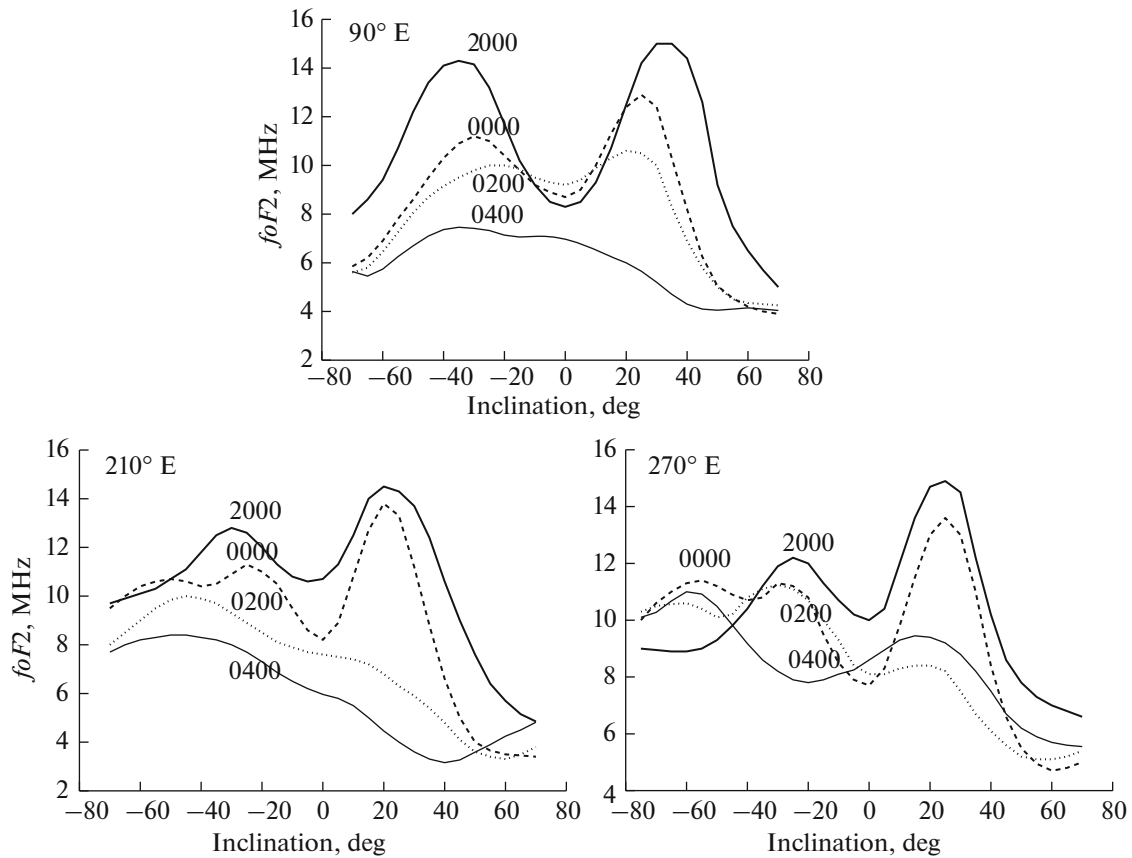


Fig. 8. Latitudinal profiles of  $foF2$  for 2000, 2200, 0200, and 0400 LT in longitudinal sectors of 90°, 210°, and 270°.

clear that this occurs after the direction of the vertical plasma drift velocity changes and the fountain effect is activated. However, as shown above and on the middle panel in Fig. 10, there is currently only a winter northern crest in the Asian longitudinal sector, while the EA at 0800 LT is not developed at all in the American sector; therefore, the EAI was set equal to 1. At 1000 LT, both EA crests are already observed in both longitudinal sectors, after which the EAI grows and reaches a local day-time peak at 1200 LT. This maximum certainly is related (with a quite explainable delay) to the local maximum of the plasma drift velocity at 1000 LT. This maximum more clearly manifests itself in the Asian sector (Matuura, 1981). The EAI midday maximum is associated with the midday decrease in  $foF2$ , which is observed as the so-called “bite-out” at the India longitudes (Rao, 1963).

The EAI decreases by 1600 LT, after which it reaches the maximum at  $\sim 2000$  LT, at first slowly and then very rapidly. This maximum is observed with a delay of 1.5–2.0 h after the evening burst of the vertical plasma drift velocity, and it is higher in the Asian sector. The EAI value then drops by 0400 LT, but a local maximum in the EAI is observed in the American sector at midnight, as already noted above. This small maximum is associated with the longitudinal effect in

the Southern hemisphere, where the  $foF2$  is maximum at the longitudes of 270°–300° around the midnight hours in a large range of latitudes, including the maximum of the southern crest. The longitudinal effect at the mid-latitudes is caused mainly by the action of neutral wind. Thus, this enhancement of EAI is associated not with an increase in the fountain effect but with effect of neutral wind. The development (resurgence) of EA crests was also noted in other studies. Thus, Walker et al. (1994) stated that it takes place at 0300 LT in the Asian sector in any season under high solar activity. Yizengaw et al. (2009) observed according to the TEC TOPEX data at 80° W for April 27, 2003, an EA minimum at 2330 LT, while the well-developed EA was observed up to 0400 LT. According to IK-19 data for the equinox, a shifting of anomaly crests from the equator was also observed, which increased its intensity (Karpachev, 2018).

The middle panel in Fig. 10 shows the diurnal  $foF2$  variations above the equator and in both anomaly crests in the longitudinal sector of 120°. The  $foF2$  values above the geomagnetic equator are 6.5–7.0 MHz at 0400–0600 LT, about 11 MHz in day-time and  $\sim 8$  MHz in the evening. The  $foF2$  values in EA crests during the day and in the evening reaches 14–15 MHz; in this

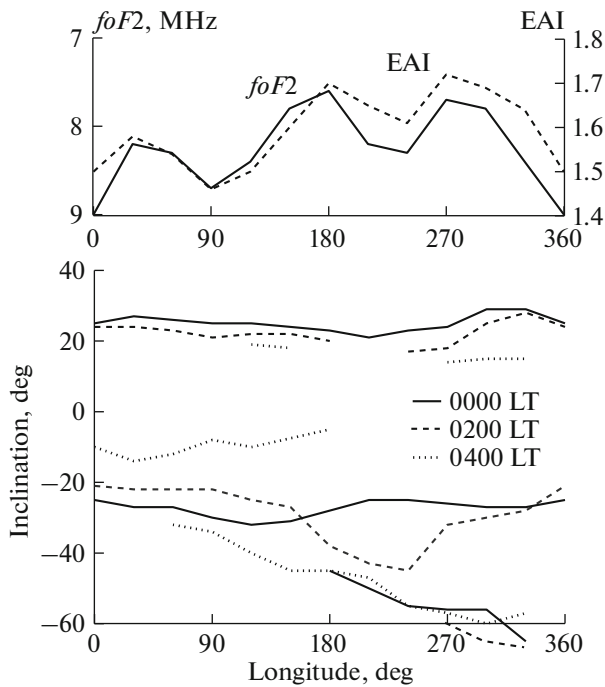


**Fig. 9.** Top: longitudinal variations and EAI for 0000 LT. Bottom: longitudinal variations in the crest positions ( $foF2$  maxima) for 0000, 0200, and 0400 LT.

case, they are slightly higher in the winter crest as compared to the summer one.

The bottom panel in Fig. 10 depicts the averaged positions of the anomaly crests for all longitudes. As already noted above, the southern summer crest is located a few degrees farther from the equator than the northern winter one; the asymmetry is not very strong. The crests move far from the equator at 2000–2200 LT, with a total width of  $\sim 60^\circ I$ . The dynamics of northern winter crest is standard: during the EA development, it moves away from the equator, while it shifts towards the equator during the decay. The dynamics of the southern crest is generally the same, but it begins to manifest itself at 0800 LT at a latitude of  $-45^\circ I$  and is actually the midlatitude  $foF2$  maximum at this time. This maximum then smoothly transfers to the “normal” crest; therefore their dynamics is presented in Fig. 10 with a single curve.

## 7. DISCUSSION

This paper concludes the analysis of  $foF2$  variations in the EA area based on data from the Interkosmos-19 satellite for high solar activity in the period of equinox, summer, and winter solstices. Each season is characterized by its own specific features. We highlight the main characteristics of the pattern for winter solstice. In winter conditions, the winter northern crest of anomaly first begins to form at 0800 LT. The summer southern crest appears much later, while the formed

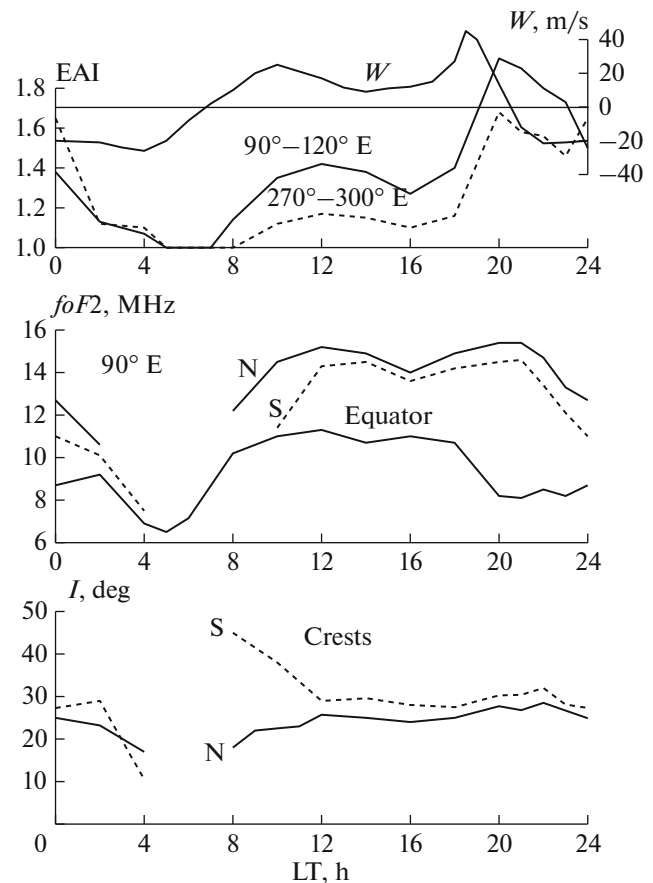


**Fig. 10.** Top: variations in the vertical plasma-drift velocity (Fejer et al., 2008) and the EAI at longitudes of  $120^\circ$  (solid curve) and longitudes of  $300^\circ$  (dashed curve). Middle: diurnal  $foF2$  variations at a longitude of  $90^\circ$  above the equator, as well as at the maximum of the northern (N) and southern (S) crests. Bottom: variations in the all-longitude average position of EA crests in the Northern and Southern Hemispheres.

EA is well pronounced for all longitudes only by 1000–1100 LT. A local day-time maximum in the EA development is observed at 1200 LT. It is related to the day-time maximum of the vertical plasma drift velocity  $W$ . The main evening EA maximum is reached at 2000 LT, 1.5–2.0 h after the evening burst of the vertical plasma drift velocity. After the reversal of the drift velocity downwards, it maintains the EA crests at the highest level for a long time. Hence, the EA is still sufficiently well-developed even at midnight, in contrast to situation at low solar activity. The EA decays by 0400 LT and is completely absent in the period of 0500–0700 LT, as in other seasons.

The  $foF2$  values above the equator undergo rather strong variations with longitude. In the afternoon and evening, they are determined mainly by variations in the vertical plasma drift velocity. In contrast to the other seasons, three harmonics are observed in the longitudinal  $foF2$  variations in this case at midday: two in the eve-

ning and three again at midnight. This is associated with the influence of the lower atmosphere on the ionospheric  $E$  region and, consequently, also on the vertical drift (e.g., Pancheva and Mukhtarov, 2012 and references therein).

The EAI variations are determined almost completely by the  $foF2$  variations above the geomagnetic equator. In the morning the EA is most developed in the Asian sector ( $90^\circ$ ), less developed in the Pacific Ocean sector ( $210^\circ$ ), and least developed in the American sector ( $300^\circ$ ). In the evening the EA is, as before, most developed in the Asian sector, less developed in the American sector, and least developed in the Pacific Ocean sector. Finally, the EA at midnight, conversely, is not very strongly developed in the Asian sector, more strongly developed in the Pacific Ocean sector, and even more strongly developed in the American-Atlantic sector ( $270^\circ$ – $300^\circ$ ). These results unite numerous discussions of EA development with local time in different longitudinal sectors.

The winter crest during the day-time and evening slightly exceeds the summer crest in magnitude; after midnight, conversely, the winter crest decays faster than the summer one. The average (for all longitudes) position of the winter crest in the day-time is  $\sim 25^\circ I$ , while the average position of the summer crest is  $\sim 30^\circ I$ . Thus, a not very strong asymmetry is observed in both the position of crests and their magnitude. The crests are at the greatest distance from the equator at 2000–2200 LT, and the anomaly width at this time is  $\sim 60^\circ I$ .

The summer southern crest in the period of EA development, as well as the northern one during the summer solstice (Karpachev, 2020), forms on the background of the midlatitude  $foF2$  maximum, which is probably associated with the neutral wind. A specific feature of the EA decay period during the winter solstice is the dynamics of the summer southern crest of anomaly and the  $foF2$  maximum, which is related to the WSA. The dynamics is so complicated that it usually raises many questions (e.g., Horvath and Essex, 2003).

## 8. CONCLUSIONS

Thus, the most complete pattern of diurnal EA development for all longitudes under conditions of high solar activity was created. This pattern cannot be considered to be finished, since a number of problems remain to be studied. For example, the process of the summer crest formation against the background of the midlatitude  $foF2$  maximum clearly needs additional analysis. The results will be taken as the basis for an empirical model of the  $foF2$  of the equatorial ionosphere, which is more adequate than the international model IRI. The model will be completed as soon as possible and will be available on the IZMIRAN website. A similar pattern of EA dynamics can also be created for conditions of low solar activity, since the experimental basis for this was recently obtained. This

will make it possible to compare in detail the EA characteristics for different seasons and at different solar activities in order to obtain a deeper understanding of mechanisms of the equatorial ionosphere formation.

## FUNDING

This work was supported by the Presidium of the Russian Academy of Sciences (Program No. 28) and the Ministry of Education and Science of the Russian Federation (Project KP 19-270).

## REFERENCES

- Balan, N. and Bailey, G.J., Equatorial plasma fountain and its effects: Possibility of an additional layer, *J. Geophys. Res.*, 1995, vol. 100, no. 11, pp. 21421–21432. <https://doi.org/10.1029/95JA01555>
- Bellchambers, W.H. and Piggott, W.R., Ionospheric measurements made at Halley Bay, *Nature*, 1958, vol. 182, pp. 1596–1597. <https://doi.org/10.1038/1821596a0>
- Chen, Y., Liu, L., Le, H., Wan, W., and Zhang, H., Equatorial ionization anomaly in the low-latitude topside ionosphere: Local time evolution and longitudinal difference, *J. Geophys. Res.*, 2016, vol. 121, pp. 7166–7182. <https://doi.org/10.1002/2016JA022394>
- Eccles, D. and King, J.W., A review of topside sounder studies of the equatorial ionosphere, *Proc. IEEE*, 1969, vol. 57, no. 6, pp. 1012–1018. <https://doi.org/10.1109/PROC.1969.7145>
- Fejer, B.G., Jensen, J.W., and Su, S.-Y., Quiet time equatorial f region vertical plasma drift model derived from ROCSAT-1 observations, *J. Geophys. Res.*, 2008, vol. 113, A05304. <https://doi.org/10.1029/2007JA012801>
- Hopkins, H.D., Longitudinal variation of the equatorial anomaly, *Planet. Space Sci.*, 1972, vol. 20, no. 12, pp. 2093–2098. [https://doi.org/10.1016/0032-0633\(72\)90065-7](https://doi.org/10.1016/0032-0633(72)90065-7)
- Horvath, I. and Essex, E.A., The Weddell Sea anomaly observed with the TOPEX satellite data, *J. Atmos. Sol.-Terr. Phys.*, 2003, vol. 65, pp. 693–706. [https://doi.org/10.1016/S1364-6826\(03\)00083-X](https://doi.org/10.1016/S1364-6826(03)00083-X)
- Huang, Y.-N. and Cheng, K., Solar cycle variations of the equatorial ionospheric anomaly in total electron content in the Asian region, *J. Geophys. Res.*, 1996, vol. 101, no. 11, pp. 24513–24520. [https://doi.org/10.1016/0021-9169\(94\)00147-G](https://doi.org/10.1016/0021-9169(94)00147-G)
- Jackson, J.E., The reduction of topside ionograms to electron-density profiles, *Proc. IEEE*, 1969, vol. 57, no. 6, pp. 960–976. <https://doi.org/10.1109/PROC.1969.7140>
- Karpachev, A.T., Characteristics of the global longitudinal effect in a nighttime equatorial anomaly, *Geomagn. Aeron.*, 1988, vol. 28, no. 1, pp. 46–49.
- Karpachev, A.T., Diurnal and longitudinal variations of the structure of an equatorial anomaly during equinoxes according to Intercosmos-19 satellite data, *Geomagn. Aeron. (Engl. Transl.)*, 2018, vol. 58, no. 3, pp. 407–419. <https://doi.org/10.1134/S0016793218030076>

- Karpachev, A.T., Variations in the structure of the equatorial anomaly during the summer solstice according to the Interkosmos-19 satellite, *Geomagn. Aeron. (Engl. Transl.)*, 2020, vol. 60, no. 2, pp. 224–235. <https://doi.org/10.1134/S0016793220020061>
- Karpachev, A.T., Gasilov, N.A., and Karpachev, O.A., Morphology and causes of the Weddell Sea anomaly, *Geomagn. Aeron. (Engl. Transl.)*, 2011, vol. 51, no. 6, pp. 812–824.
- Kil, H., Oh, S.-J., Paxton, L.J., and Fang, T.-W., High-resolution vertical  $e^{\pm}$  drift model derived from rocsat-1 data, *J. Geophys. Res.*, 2009, vol. 114, p. A10314.
- King, J.W., Airglow observations and the decay of the ionospheric equatorial anomaly, *J. Atmos. Terr. Phys.*, 1968, vol. 30, pp. 391–402. [https://doi.org/10.1016/0021-9169\(68\)90110-4](https://doi.org/10.1016/0021-9169(68)90110-4)
- King, J.W., Olatunji, E.O., Eccles, D., and Newman, W.S., The integrated electron content in the equatorial ionosphere, *J. Atmos. Terr. Phys.*, 1967, vol. 29, no. 11, pp. 1391–1396. [https://doi.org/10.1016/0021-9169\(67\)90230-9](https://doi.org/10.1016/0021-9169(67)90230-9)
- Klimenko, M.V., Klimenko, V.V., Karpachev, A.T., Ratovsky, K.G., and Stepanov, A.E., Spatial features of Weddell Sea and Yakutsk anomalies in  $foF_2$  diurnal variations during high solar activity periods: Interkosmos-19 satellite and ground-based ionosonde observations, IRI reproduction and GSM tip model simulation, *Adv. Space Res.*, 2015, vol. 55, no. 8, pp. 2020–2032. <https://doi.org/10.1016/j.asr.2014.12.032>
- Lei, J., Thayer, J.P., and Forbes, J.M., Longitudinal and geomagnetic activity modulation of the equatorial thermosphere anomaly, *J. Geophys. Res.*, 2010, vol. 115, A08311. <https://doi.org/10.1029/2009JA015177>
- Liu, H. and Watanabe, S., Seasonal variation of the longitudinal structure of the equatorial ionosphere: Does it reflect tidal influences from below?, *J. Geophys. Res.*, 2008, vol. 113, A08315. <https://doi.org/10.1029/2008JA013027>
- Liu, H., Stolle, C., Forster, M., and Watanabe, S., Solar activity dependence of the electron density at 400 km at equatorial and low latitudes observed by CHAMP, *J. Geophys. Res.*, 2007, vol. 112, A11311. <https://doi.org/10.1029/2007JA012616>
- Lockwood, G.E.K. and Nelms, G.L., Topside sounder observations of the equatorial anomaly in the 75°W longitude zone, *J. Atmos. Terr. Phys.*, 1964, vol. 26, no. 5, pp. 569–580. [https://doi.org/10.1016/0021-9169\(64\)90188-6](https://doi.org/10.1016/0021-9169(64)90188-6)
- Lyon, A.J. and Thomas, L., The  $F_2$ -region equatorial anomaly in the African, American and East Asian sectors during sunspot minimum, *J. Atmos. Terr. Phys.*, 1963, vol. 25, no. 7, pp. 373–386. [https://doi.org/10.1016/0021-9169\(63\)90170-3](https://doi.org/10.1016/0021-9169(63)90170-3)
- Matuura, N., Characteristics of global distribution of  $foF_2$ , *Sol. Terr. Environ. Res. Jpn.*, 1981, vol. 5, pp. 35–38.
- Oh, S.-J., Kil, H., Kim, W.-T., Paxton, L.J., and Kim, Y.H., The role of the vertical  $E \times B$  drift for the formation of the longitudinal plasma density structure in the low-latitude  $F$  region, *Ann. Geophys.*, 2008, vol. 26, no. 7, pp. 2061–2067. <https://doi.org/10.5194/angeo-26-2061-2008>
- Pancheva, D. and Mukhtarov, P., Global response of the ionosphere to atmospheric tides forced from below: Recent progress based on satellite measurements global tidal response of ionosphere, *Space Sci. Rev.*, 2012, vol. 168, nos. 1–4, pp. 175–209. <https://doi.org/10.1007/s11214-011-9837-1>
- Rajaram, G., Structure of the equatorial  $F$ -region, topside and bottomside—a review, *J. Atmos. Terr. Phys.*, 1977, vol. 39, no. 9, pp. 1125–1144. [https://doi.org/10.1016/0021-9169\(77\)90021-6](https://doi.org/10.1016/0021-9169(77)90021-6)
- Ram, S.T., Su, S.-Y., and Liu, C.H., FORMOSAT-3/COSMIC observations of seasonal and longitudinal variations of equatorial ionization anomaly and its interhemispheric asymmetry during the solar minimum period, *J. Geophys. Res.*, 2009, vol. 114, A06311. <https://doi.org/10.1029/2008JA013880>
- Rao, B.C.N., Some characteristic features of the equatorial ionosphere and the location of the  $F$ -region equator, *J. Geophys. Res.*, 1963, vol. 68, no. 9, pp. 2541–2549. <https://doi.org/10.1029/JZ068i009p02541>
- Rao, C.S.R. and Malthotra, P.L., A study of geomagnetic anomaly during I.G.Y., *J. Atmos. Terr. Phys.*, 1964, vol. 26, no. 11, pp. 1075–1085. [https://doi.org/10.1016/0021-9169\(64\)90093-5](https://doi.org/10.1016/0021-9169(64)90093-5)
- Rastogi, R.G., Chandra, H., Sharma, R.P., and Rajaram, G., Ground-based measurements of ionospheric phenomena associated with the equatorial electrojet, *Indian J. Radio Space Phys.*, 1972, vol. 1, no. 2, pp. 119–135.
- Rush, C.M., Rush, S.V., Lyons, L.R., and Venkateswaran, S.V., Equatorial anomaly during a period of declining solar activity, *Radio Sci.*, 1969, vol. 4, no. 9, pp. 829–841. <https://doi.org/10.1029/RS004i009p00829>
- Sastri, J.H., Equatorial anomaly in  $F$ -region—a review, *Indian J. Radio Space Phys.*, 1990, vol. 19, no. 4, pp. 225–240.
- Sharma, R.P. and Hewens, E.J., A study of the equatorial anomaly at American longitudes during sunspot minimum, *J. Atmos. Terr. Phys.*, 1976, vol. 38, no. 5, pp. 475–484. [https://doi.org/10.1016/0021-9169\(76\)90004-0](https://doi.org/10.1016/0021-9169(76)90004-0)
- Thomas, L., The  $F_2$ -region equatorial anomaly during solstice periods at sunspot maximum, *J. Atmos. Terr. Phys.*, 1968, vol. 30, no. 9, pp. 1631–1640. [https://doi.org/10.1016/0021-9169\(68\)90011-1](https://doi.org/10.1016/0021-9169(68)90011-1)
- Tsai, L.-C., Liu, C.H., Hsiao, T.Y., and Huang, J.Y., A near real-time phenomenological model of ionospheric electron density based on GPS radio occultation data, *Radio Sci.*, 2009, vol. 44, RS5002. <https://doi.org/10.1029/2009RS004154>
- Walker, G.O., Longitudinal structure of the  $F$ -region equatorial anomaly—a review, *J. Atmos. Terr. Phys.*, 1981, vol. 43, no. 8, pp. 763–774. [https://doi.org/10.1016/0021-9169\(81\)90052-0](https://doi.org/10.1016/0021-9169(81)90052-0)
- Walker, G.O. and Chen, C.S., The diurnal variation of the equatorial anomaly in the topside ionosphere at sunspot maximum, *J. Atmos. Sol.-Terr. Phys.*, 1976, vol. 38, no. 7, pp. 699–706. [https://doi.org/10.1016/0021-9169\(76\)90108-2](https://doi.org/10.1016/0021-9169(76)90108-2)



- Walker, G.O., Ma, J.H.K., and Golton, E., The equatorial ionospheric anomaly in electron content from solar minimum to solar maximum for South East Asia, *Ann. Geophys.*, 1994, vol. 12, nos. 2–3, pp. 195–209. <https://doi.org/10.1007/s00585-994-0195-0>
- Yizengaw, E., Moldwin, M.B., Sahai, Y., and Rodolfo, J., Strong postmidnight equatorial ionospheric anomaly observations during magnetically quiet periods, *J. Geophys. Res.*, 2009, vol. 114, A12308. <https://doi.org/10.1029/2009JA014603>
- Yue, X., Schreiner, W.S., Kuo, Y.-H., and Lei, J., Ionosphere equatorial ionization anomaly observed by GPS radio occultations during 2006–2014, *J. Atmos. Sol.-Terr. Phys.*, 2015, vol. 129, no. 7, pp. 30–40. <https://doi.org/10.1016/j.jastp.2015.04.004>
- Zeng, Z., Burns, A., Wang, W., Lei, J., Solomon, S., Syndergaard, S., Qian, L., and Kuo, Y.-H., Ionospheric annual asymmetry observed by the cosmic radio occultation measurements and simulated by the TIEGCM, *J. Geophys. Res.*, 2008, vol. 113, A07305. <https://doi.org/10.1029/2007JA012897>
- Zhao, B., Wan, W., Liu, L., and Ren, Z., Characteristics of the ionospheric total electron content of the equatorial ionization anomaly in the Asian–Australian region during 1996–2004, *Ann. Geophys.*, 2009, vol. 27, no. 10, pp. 3861–3873. <https://doi.org/10.5194/angeo-27-3861-2009>

*Translated by M. Samokhina*